

PAPER • OPEN ACCESS

## Waste to wealth: a solution to textile dyes related pollution

To cite this article: Boya Palajonnala Narasaiah and Badal Kumar Mandal 2020 *Mater. Res. Express* 7 024001

### Recent citations

- [Structure, morphological, dielectric and mechanical properties of biopolymer blends](#)  
S.N.M. Shareef

View the [article online](#) for updates and enhancements.



**The Electrochemical Society**  
Advancing solid state & electrochemical science & technology  
2021 Virtual Education

**Fundamentals of Electrochemistry:**  
Basic Theory and Kinetic Methods  
Instructed by: **Dr. James Noël**  
Sun, Sept 19 & Mon, Sept 20 at 12h–15h ET

**Register early and save!**



# Materials Research Express



## PAPER

# Waste to wealth: a solution to textile dyes related pollution

### OPEN ACCESS

#### RECEIVED

11 November 2019

#### REVISED

8 January 2020

#### ACCEPTED FOR PUBLICATION

15 January 2020

#### PUBLISHED

17 February 2020

Original content from this work may be used under the terms of the [Creative Commons Attribution 4.0 licence](#).

Any further distribution of this work must maintain attribution to the author(s) and the title of the work, journal citation and DOI.



Boya Palajonnala Narasaiah and Badal Kumar Mandal

Department of Chemistry, School of Advanced Sciences, Vellore Institute of Technology, Vellore-14, Tamil Nadu, India

E-mail: [badalmandal@vit.ac.in](mailto:badalmandal@vit.ac.in) and [badalkmandal@gmail.com](mailto:badalkmandal@gmail.com)

**Keywords:** agro-waste durva grass extract, ZnO NPs, Photocatalytic activity, antioxidant activity

Supplementary material for this article is available [online](#)

## Abstract

This study describes biosynthesis of Zinc oxide nanoparticles (ZnO NPs) using agro-waste durva grass aqueous extract without uses of any hazardous chemicals and stabilizing agents. Surface plasmon resonance (SPR) band of the synthesized ZnO NPs confirmed its conversion from its metal salt to NPs by UV–vis spectroscopy. Characterization of functional groups in durva grass aqueous extract and ZnO NPs surfaces were identified by Fourier transform infrared spectroscopy (FTIR), purity and crystallinity by power x-ray diffraction analysis (XRD), size and morphology by transmission electron microscopy analysis (TEM), elemental composition by Energy Dispersive x-ray spectroscopy (EDAX), stability by thermogravimetric analysis (TGA) and dynamic light scattering (DLS) study. The synthesized ZnO NPs was highly stable with average particle size of 17 nm. The photocatalytic activity of ZnO NPs was studied under UV irradiation to methylene blue (MB) and methyl orange (MO) degradation ( $10 \text{ mg l}^{-1}$  each). 98.1% of MB was degraded within 60 min, while 97.5% of MO within 100 min. In addition, antioxidant activity of ZnO NPs showed 91.8% free radical scavenging capacity at the dose of  $250 \text{ mg l}^{-1}$  which implies its importance in biomedical applications.

## Introduction

Nanotechnology is a fast growing arena in science and technology while nanomaterials having improved optical, magnetic and electrical properties compare to bulk materials are the promising materials in all these fields. Synthesis of nanomaterials has been widely studied in nanoscience due to enhanced physicochemical properties which leads to promising uses in different fields such as medicines, food sciences, agricultural pesticides, environmental clean-up, and nanocatalyst in organic synthesis, chemical reduction, biosensors and pollutants degradation [1, 2].

Synthesis of metal oxide nanomaterials (MONPs) by different methods i.e. solvothermal method [3], hydrothermal method [4], precipitation method [5], sol-gel method [6] and thermal decomposition [7] needs toxic chemical and solvent as well as toxic stabilizing agents [8, 9]. Effectively these methods can tune the shape and size of nanoparticles, but all these methods are expensive and required high temperature, pressure and energy. Now-a-days environmentally friendly MONPs are synthesized using simple green technologies and widely used in different applications such as photocatalytic degradation of water pollutants, nanocatalyst in synthesising organic compounds and biomedical application [10–12]. A few published articles have described the synthesis of ZnO nanoparticles (ZnO NPs) using green route [13, 14]. Niranjan Bala *et al* [13] reported the biosynthesis of ZnO NPs by using *Hibiscus subdariffa* leaf extract, whereas Sundrarajan *et al* [14] synthesized ZnO NPs by using *Pongamia pinnata* leaf extract.

Organic dyes are used extensively by different industries which are well known toxicants to environment and ecosystem [15]. Moreover water containing dye of  $1 \text{ mg l}^{-1}$  is hazardous to environments and dyes contaminated wastewater is carcinogenic to human beings. Hence elimination of hazardous MB, MO and RB dyes from waste water is a challenging task to the scientists [16]. The international environmental standards have become more stringent day by day towards these pollutants.

Several methods have been used for wastewater treatment and degradation of organic pollutants which are Fenton oxidation, chemical coagulation, aerobic, anaerobic, chemical oxidation, adsorption, membrane separation, electrochemical treatment, ion exchange and reverse osmosis [17, 18]. These techniques have some drawbacks and hence lower cost & safer technologies are still needed for the practical applications. Among them, advanced catalytic degradation finds some importance in degrading pollutants of wastewater generated from industrial and living sources. Presently, nanocatalysts have undergone an enormous growth and seem to be an intensifying smart material in the field of remediation of environmental pollutants [19]. Not a single method is adequate to degrade highly stable aqueous dyes. Therefore it warrants effective remove methods for water contaminants. Among them photodegradation is the best alternative method to the conventional methods for remediation of toxic and hazardous pollutants from water and wastewater [20–22].

In the present study synthesise ZnO NPs using agro-waste durva grass aqueous extract was planned for the first-time, characterized by different instrumental techniques and finally its applications to environmentally harmful MB and MO dye degradation and antioxidant study using DPPH assay against standard antioxidant ascorbic acid were performed.

## Experimental methods

### Materials

Fresh durva grass was collected from sunflower crop field at Chilakaladona village, Mantralayam Mandal, Kurnool District, Andhra Pradesh, India. Zinc acetate dihydrate  $Zn(O_2CCH_3)_2 \cdot 2(H_2O)$ , organic dyes such of methylene blue (MB) and methyl orange (MO) were purchased from Sigma-Aldrich, India. Milli-Q water was used in this project.

### Collecting material and preparation of durva grass extract

The green durva grass was collected, cleaned with water and after thorough washing durva grass was cut into small pieces. After hot water washing the durva grass pieces were dried at room temperature over night. The dried durva grass was powdered and sieved by 100 mesh sieve. 3 gm powder was added to 100 ml distilled water and then boiled in a water bath at 100 °C for 30 min to prepare the aqueous extract. The cooled aqueous extract was filtered through Whatman filter paper and then the filtrate was used for the synthesis of ZnO NPs.

### Synthesis of zinc oxide nanoparticles

About 0.329 gm of zinc acetate dihydrate  $Zn(O_2CCH_3)_2 \cdot (H_2O)_2$  (0.05 M) was dissolved in 30 ml double distilled water and then 30 ml durva grass aqueous extract was added dropwise with stirring thoroughly at 80 °C for 3h. The solution colour changed from light green to brown after 10 min heating due to the surface Plasmon resonance indicating the formation of ZnO NPs. The cooled reaction mixture was centrifuged at 5000 rpm for 30 min and the obtained precipitation was washed thrice with absolute ethanol followed by double distilled water, dried on hot air oven. The resulting dried powder was pulverized and heated at 500 °C for 3h inside a furnace. The obtained calcined ZnO NPs was subjected to characterization followed by applications.

### Test for phenolic compounds

#### *Qualitative determination of phenolic compounds by phenols- Ferric Chloride test*

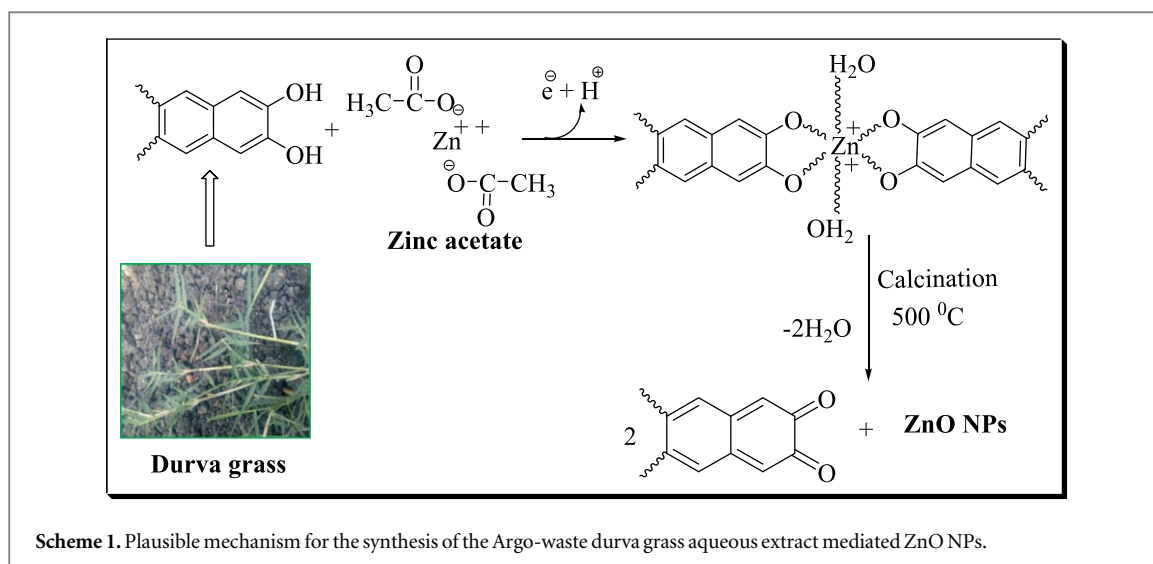
A few drops of 5% neutral  $FeCl_3$  solution was mixed with 3 ml durva grass extract and the appearance of intense dark green color indicated the participation of phenolic groups in the durva grass extract.

#### *Quantitative determination of phenols-FC reagent test*

Total phenolic content in Agro-waste durva grass aqueous extract was measured using Folin-Ciocalteu (FC) reagent with the help of UV-vis spectrophotometer. In briefly, 1 ml extract was added with 2 ml FC reagent (10%) and then 4 ml sodium carbonate solution (5%) was added. The absorbance of the reaction mixture (intense dark green colour) was monitored by spectrophotometer. Standard gallic acid was used as standard for phenolic content, The total phenolic contents in the plant extracts is expressed in terms of gallic acid equivalent (the standard curve equation:  $y = 0.004X - 0.0753$ ) and it is found to be  $81.45 \text{ mg g}^{-1}$ . The plausible mechanism of ZnO NPs synthesis using durva grass aqueous extracts is shown in scheme 1.

### Characterisation of ZnO NPs

The optical properties of ZnO NPs were characterized by using UV-visible spectroscopy. ZnO NPs was dispersed in water by using ultrasonic bath (Enertech ultrasonic bath) for 20 min and then was analysed for absorbance at room temperature using UV-visible (Shimadzu UV-2450). The functional groups of capped phytochemicals from durva grass extract on ZnO NPs surfaces were identified by Attenuated Total



Reflection-Fourier Transform Infra-Red (FT-IR) spectroscopy (JASCO ATR-FT-IR 4100) against durva grass powder as control in wave number range of  $500\text{--}4100\text{ cm}^{-1}$  at a resolution of  $4\text{ cm}^{-1}$  using potassium bromide pellets. The bandgap energy ( $E_g$ ) of ZnO NPs was determined by using UV-vis-NIR spectrophotometer (JASCO V-670). The x-ray diffractogram (powder XRD, Bruker D8 advance) of ZnO NPs was taken by x-ray diffraction analysis after coating ZnO NPs onto XRD grid and spectra were recorded for the  $2\theta$  values of  $10^\circ\text{--}90^\circ$  with a scanning rate of  $4^\circ\text{ min}^{-1}$ . The powder x-ray diffractometer used  $\text{CuK}\alpha$  radiation with a  $\lambda_{\text{max}}$  of  $1.54\text{ \AA}$ .

The size and shape of the prepared ZnO NPs were checked by dispersing sample dispersion on Cu grid by HR-TEM (JEOL JEM 2100 USA) with  $0.1\text{ nm}$  resolution and acceleration voltage of  $200\text{ keV}$ . The elemental composition of ZnO NPs was analysed by energy dispersive x-ray (EDX) analysis. The electrophoretic mobility of the samples was analysed by Nano partitici (SZ-100 i.e. DLS) instrument in checking sedimentation of the NPs based on the charge distribution. In addition, the stability of the ZnO NPs was analysed by thermogravimetric analysis (2100F - TGA-JOEL). Its acceleration voltage was  $100\text{ kV}$ .

#### Catalytic activity of ZnO NPs

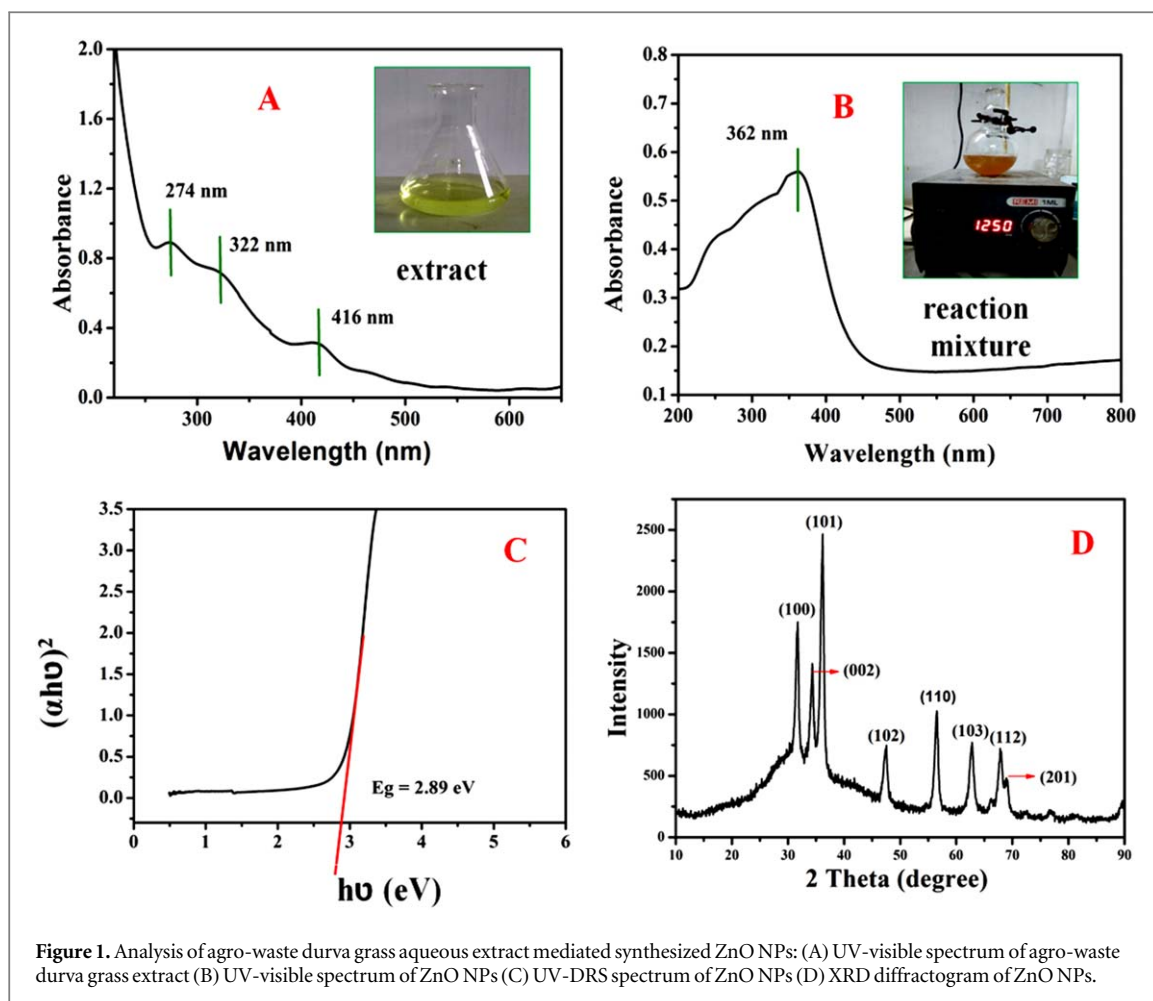
Degradation of MB and MO dyes by photocatalyst ZnO NPs was carried out using Heber photoreactor (Heber photoreactor HML MP 88) attached mercury lamp ( $0.170\text{ \AA}$ ,  $8\text{ W}$ ,  $220\text{--}230\text{ V}$  at  $50\text{ Hz}$ ) with UV exposure ( $254\text{ nm}$ ). Basically,  $60\text{ ml}$  of MB and MO dye aqueous solution ( $10\text{ mg l}^{-1}$ ) was taken in a quartz tube and ZnO NPs ( $20\text{ mg}$ ) was added with stirring for  $30\text{ min}$  in the dark condition without UV-light exposure. In a similar way effects of varying catalyst and dye concentration were studied on the degradation of MB and MO dyes. The progress of degradation process was monitored using UV-visible spectroscopy by collecting samples time to time and measuring absorbance of the collected solution.

#### Antioxidant activity of ZnO NPs by DPPH assay

The antioxidant activity of ZnO NPs ( $50, 100, 150, 200, 250\text{ mg l}^{-1}$ ) was checked after mixing in  $1\text{ ml}$  methanol solution of DPPH ( $50\text{ mg l}^{-1}$ ) in  $2\text{ ml}$  Eppendorf tube for incubation at  $37^\circ\text{ C}$  for  $30\text{ min}$  in dark. The colour change (purple to yellow) was monitored by a UV-visible spectrophotometry at  $\lambda_{\text{max}} 517\text{ nm}$  in triplicate against std. ascorbic acid as reference antioxidant. The free radical scavenging capacity (%) of ZnO NPs was calculated as: Inhibition (%) of DPPH Scavenging activity =  $[(A_0 - A_t) * 100] / A_0$  Where,  $A_0$  is absorbance value of control sample (DPPH) and  $A_t$  is absorbance value of the test sample (DPPH + ZnO NPs) at time 't'.

## Results and discussion

Absorption spectrum of agro-waste durva grass aqueous extract shows three absorption peaks at  $274\text{ nm}$ ,  $322\text{ nm}$  and  $416\text{ nm}$  due to  $\pi \rightarrow \pi^*$  transitions (figure 1(A)). These absorption peaks may develop due to the presence of phytochemicals in the aqueous extract [23]. Normally polyphenolic, carboxylic and nitrile compounds appear at  $270\text{--}274\text{ nm}$  in the absorption spectrum. Formation of ZnO NPs turned solution colour from yellow to brown with a SPR band at  $362\text{ nm}$  by spectroscopy (figure 1(B)). Similar result was reported for ZnO NPs synthesized by using tea leaf aqueous extract [24]. UV-vis diffuse reflectance spectroscopy (UV-Vis-DRS) study was carried out using pellets form of ZnO NPs to determine band gap ( $E_g$ ) value between  $200\text{--}800\text{ nm}$ . The band gap energy was calculated by using the following formula as  $(\alpha h\nu)^2 = A(h\nu - E_g)^n$



where  $\alpha$  is the absorption coefficient,  $A$  is the constant,  $h\nu$  as photon energy,  $n = 2$  for direct and  $n = \frac{1}{2}$  for indirect transition,  $E_g$  is the band gap energy. Figure 1(C) shows the graphical plot of  $h\nu$  versus  $(\alpha h\nu)^2$  and it gives the optical band gap energy of 2.89 eV which is similar to other reports [25].

X-ray diffraction (XRD) analysis was performed to investigate the crystalline nature and purity of the calcined ZnO NPs. Figure 1(D) demonstrates the XRD pattern of ZnO NPs which shows the appearance of eight characteristic diffraction peaks at  $hkl$  values of 100, 002, 101, 102, 110, 103, 112 and 201 corresponding to the reflection at  $2\theta$  values of 31.77, 33.88, 35.77, 47.44, 56.48, 62.66, 67.83 and 69.11 respectively. The lattice plane with  $hkl$  (101) value is more intense resulting small crystallite size ZnO NPs (JCPDS N0: 96-230-0451). The XRD pattern of ZnO NPs exactly matches with the Match3 software (figure S1 is available online at [stacks.iop.org/MRX/7/024001/mmedia](https://stacks.iop.org/MRX/7/024001/mmedia)). The obtained diffraction pattern corresponds to hexagonal structure of ZnO NPs ( $a = b = 3.2493 \text{ \AA}$  and  $c = 5.2057 \text{ \AA}$ ). The average crystallite size is calculated by Scherrer's equation as  $D = k\lambda/\beta\cos(\theta)$ , where  $D$ , average crystal size;  $K$ , Scherrer's coefficient (0.891);  $\lambda$ , x-ray wave length ( $\lambda = 1.5406 \text{ \AA}$ );  $\beta$ , full width at half maximum intensity (FWHM) in radians and  $\theta$ , Bragg's angle. Estimation of the crystallite size on all the planes using Scherrer's equation is depicted in table 1. The average crystallite size is 12.42 nm. Similar type of ZnO NPs was synthesized by using *Urtica dioica* L. plant leaves extract [26]. The inter-planer distance values of the synthesized ZnO NPs are presented in table 1 which shows a good agreement with standard ZnO NPs inter-planer distance values.

Figure 2(A) shows FT-IR spectrum of durva grass aqueous extract. This spectrum shows a strong absorbance peak at  $3329.14 \text{ cm}^{-1}$  which corresponds to  $-\text{OH}$  stretching vibration of hydroxyl group of polyphenols. The absorption band located at around  $2951.09 \text{ cm}^{-1}$  can be attributed to nitrile  $-\text{C}\equiv\text{N}-$  stretching vibration. The peak absorption band at  $2846.93 \text{ cm}^{-1}$  corresponds to aromatic ring  $-\text{C}-\text{H}$  stretching vibration,  $1631.78 \text{ cm}^{-1}$  band for  $-\text{N}-\text{H}$  stretching vibration of amine functional group, bands at  $1452.40-1379.10 \text{ cm}^{-1}$  for the presence of  $-\text{CH}$ ,  $-\text{CH}_2$  and  $-\text{CH}_3$  stretching vibrations, which are characteristic of alkane groups of cellulose, respectively. A small band at  $1240.45 \text{ cm}^{-1}$  could be assigned to  $-\text{C}-\text{O}-\text{C}-$  stretching vibration of ester functional group, while a weak absorption band at  $1014.56 \text{ cm}^{-1}$  is associated with the  $-\text{C}-\text{O}-\text{H}$  bending vibration and band at  $549.71 \text{ cm}^{-1}$  for  $-\text{C}-\text{H}$  bending vibration of alkane. All bands appeared within  $4000-400 \text{ cm}^{-1}$  which indicates the presence of polyphenols such as flavonoids, alkaloids and phenolic acids,

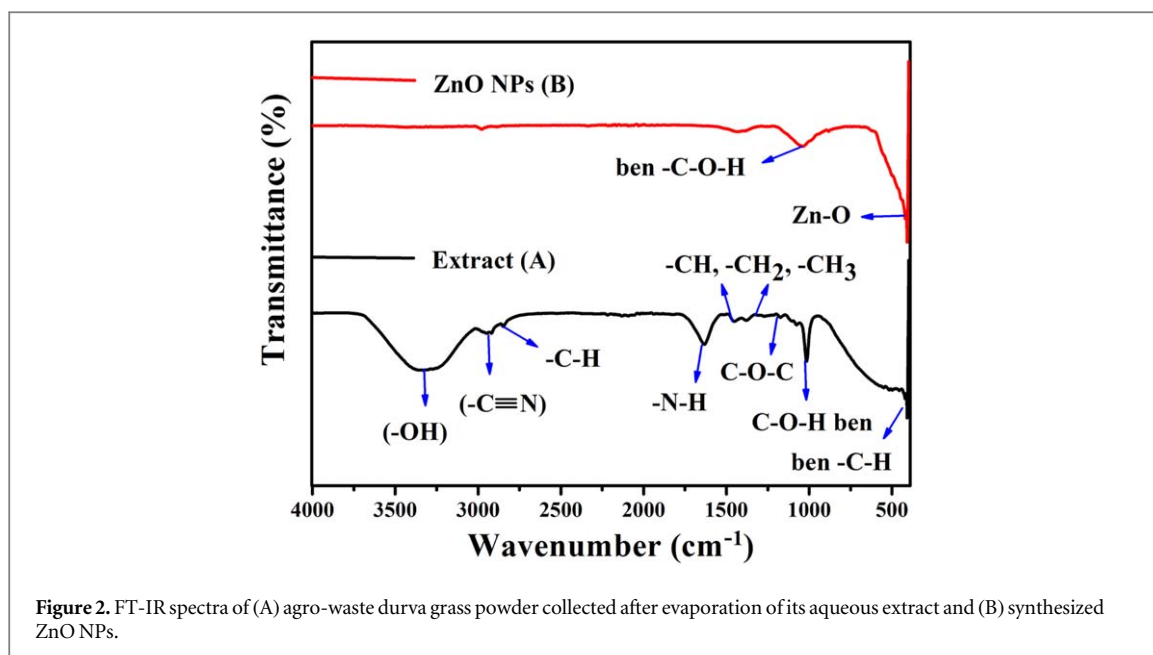


**Table 1.** The structure and geometric parameters of ZnO NPs from diffraction study.

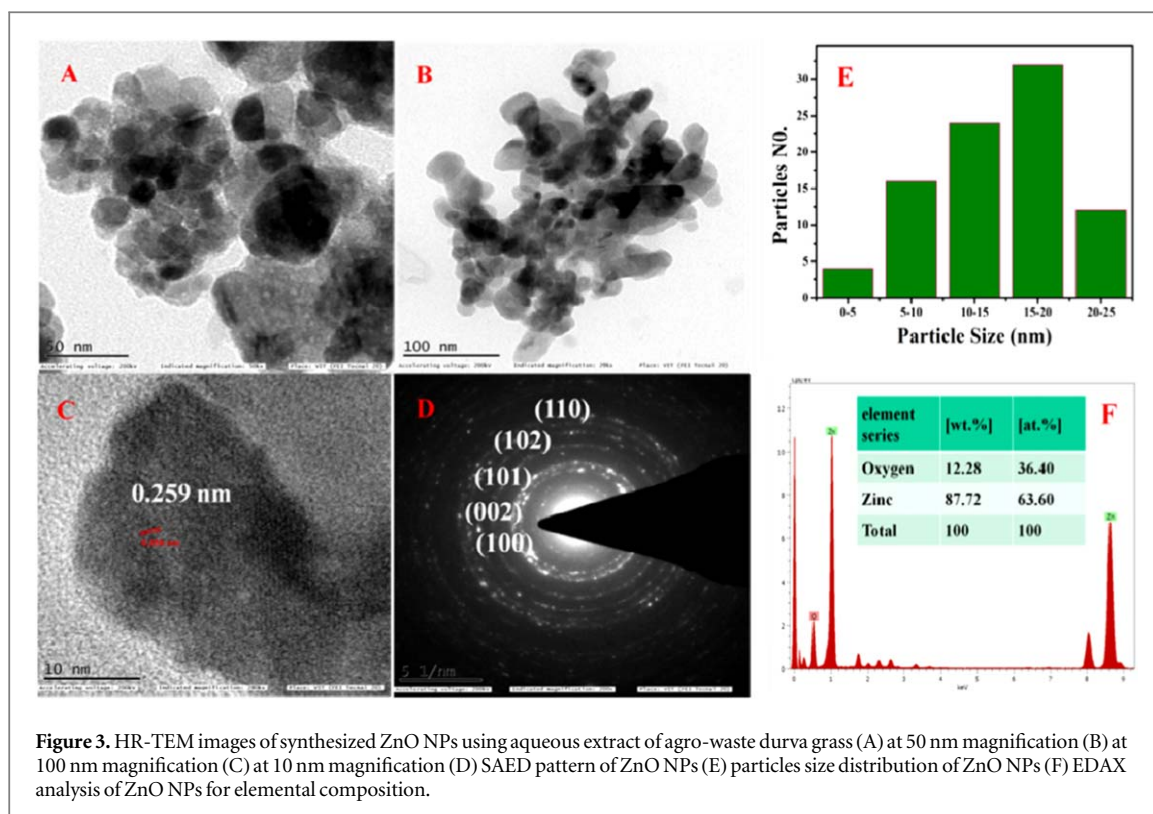
NPs	Lattice plane	2 Theta	FWHM value	d-spacing (Å)	Cos( $\theta$ )	Crystallite Size (nm)
ZnO NPs	(100)	31.77	0.58	2.85	0.9618	14.88
	(002)	33.88	0.57	2.65	0.9554	15.24
	(101)	35.77	0.67	2.52	0.9502	13.04
	(102)	47.44	0.75	1.92	0.9155	12.09
	(110)	56.48	0.73	1.63	0.8809	12.91
	(103)	62.66	0.84	1.49	0.8541	11.57
	(112)	67.83	0.86	1.38	0.8299	11.62
	(201)	69.11	1.25	1.36	0.8236	8.05
Average size					12.42 n	

cellulose, terpenoids and proteins compounds. Khodadadi *et al* [27] reported the presence of different functional groups in *Achillea millefolium* L. extract which was responsible for the synthesis of Ag NPs.

Normally plant based synthesized metal and metal oxide NPs possess higher stability due to capping of phytochemicals on their surfaces. Hence FT-IR analysis was performed to identify the possible functional groups adhere to synthesized ZnO NPs surfaces. Figure 2(B) shows the FTIR spectrum of ZnO NPs. Phytochemicals such as alkaloids, flavonoids, cellulose and phenols, proteins and polyphenols having functional groups of carboxylic acid, ketons, amines and alcohol may reduce to zinc salts to ZnO NPs. However polyphenols exhibited more active role in the biosynthesis of ZnO NPs [28]. A significant peak at  $1037.70\text{ cm}^{-1}$  is referred to  $\text{C-O-H}$  bending vibration. The new stretching vibration peak appeared at  $437.84\text{ cm}^{-1}$  corresponding to metal and oxygen (Zn-O) stretching vibration. No other peaks appeared which suggests purity of ZnO NPs.

GC-MS analysis was carried out to screen and identify phytochemicals of durva grass extract which were responsible for the formation of ZnO NPs. The two major peaks appeared at retention time of 21.32 and 22.94 min in the GC-MS chromatogram (figure S2). The 21.32 min peak indicated aliphatic ester compound and 22.94 min peak for aromatic ester compound. Other major peaks i.e. 15.52 min peak could be assigned to aromatic heterocyclic compound, the peak at 17.92 min to boron compounds, the peak at 19.82 min represent to fatty acids and the peak at 27.68 min could be assigned to aliphatic ester compounds (table S1). These compounds i.e. phytochemicals in durva grass extract were identified by matching with NIST library and could be responsible for the synthesis of ZnO NPs.

Size and morphology of synthesized ZnO NPs were checked by HR-TEM. Figures 3(A)-(C) demonstrates the TEM images of ZnO NPs at different magnifications. Figure 3(D) shows SAED pattern suggesting polycrystalline nature of ZnO NPs. The bright spots in SAED pattern indicate its crystalline nature and spots in the form of circular rings confirms polycrystalline nature of ZnO NPs. Also, results on size and lattice planes of



spherical ZnO NPs are good agreement with the XRD data [29]. The histogram of ZnO NPs shows the size range of ZnO NPs within 5–25 nm (figure 3(E)) with a mean particles size of 17.25 nm. The elemental composition of ZnO NPs was monitored by energy dispersive x-ray spectroscopy (EDAX) (figure 3(F)) which shows the characteristic signal of zinc (wt% 87.72, atomic wt% 63.60) and oxygen (Wt% 12.28, At. wt% 36.40) indicating purity of ZnO NPs. Similar results were reported by Koupaei *et al* [30] for coffee powder extract mediated synthesized ZnO NPs.

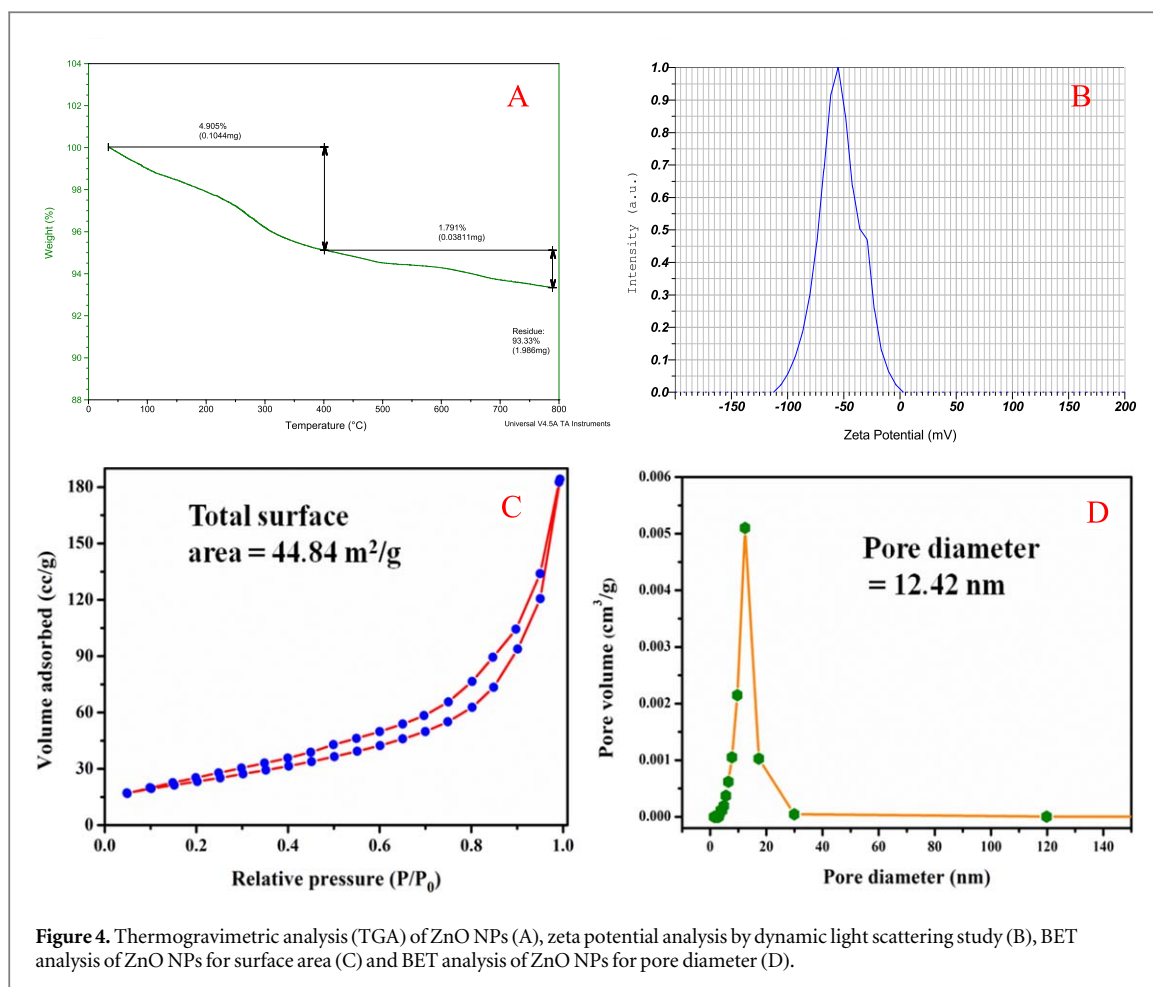
Thermogravimetric analysis (TGA) shows any loss of weight during annealing of ZnO NPs at high temperature (figure 4(A)). Total two weight losses were observed in the range of 50 °C–800 °C. Initial 4.9% of the total weight loss at 50 °C–400 °C was due to the expulsion of surface adsorbed water molecule and 2nd wt. loss (1.8%) occurred at 400 °C–800 °C, because terminal hydroxyl groups bonded to the surface of ZnO NPs were lost. No further weight loss was observed even after high temperature heating (>800 °C). Wang *et al* [31] reported a weight loss of 6.7% on heating in between 50 °C–800 °C due to removal of volatile products from ZnO NPs. All organic residues was lost after annealing at and above 500 °C and no further weight loss was there within 400 °C–800 °C in the TGA curve of ZnO NPs, but pure crystallinity was achieved by heating at 800 °C.

The dispersion stability of ZnO NPs was checked by measuring Zeta potential using photon correlation spectroscopy (PCS) i.e. dynamic light scattering (DLS) study. Figure 4(B) shows Zeta potential of –46.9 mV which describes the high stability of ZnO NPs dispersion. Similar results were reported by Suganthi *et al* [32] and Moghaddam *et al* [33]. The higher zeta potential value indicates its higher surface charge on ZnO NPs surfaces.

Photocatalytic activity of ZnO NPs depends on its surface area. Figure 4(C) shows Brunauer–Emmett–Teller (BET) analysis of ZnO NPs surface area and it is 44.84 m<sup>2</sup> g<sup>-1</sup>. Similar BET surface area of ZnO NPs was reported elsewhere as 34 m<sup>2</sup> g<sup>-1</sup> [34]. Figure 4(D) shows the Barret, Joyner and Halenda (BJH) model for pore size calculation and average pore diameter is 12.42 nm and pore volume is 0.16 cc g<sup>-1</sup>. Figure 4(C) represents the hysteresis loop of adsorption and desorption isotherm which is very similar to type IV isotherm [35]. The specific surface area of nanomaterials is correlated to its particle size in BET model by the following formula as  $S = 6/\rho d$ , where  $\rho$  is the ZnO NPs density (5.67700 g cm<sup>-3</sup>) taken from XRD analysis,  $d$  is the particles size;  $S$  is the specific surface area from BET-adsorption and desorption equilibrium (44.84 m<sup>2</sup> g<sup>-1</sup>). The average size of ZnO NPs is 23.19 nm, which is in good agreement with TEM (17.25 nm) and powder XRD (12.42 nm) results. The slight difference in particle size is because all particles are assumed to be spherical in nature by BET model.

#### Photodegradation of methylene blue (MB)

Degradation of MB dye was performed by ZnO NPs as photocatalyst under UV irradiation ( $\lambda = 254$  nm). Figure 5(A) shows degradation of MB dye within 0 min to 60 min and MB dye concentration decreased with time by UV irradiation and photocatalyst ZnO NPs. The degradation progress of MB dye was followed by



UV-vis spectrophotometer and the dye degradation (%) was calculated by using the following formula: Degradation of dye (%) =  $(C_0 - C_t) * 100 / C_0$  where,  $C_0$  is the initial concentration of dye absorbance and  $C_t$  is the concentration of dye at time 't'. Initially degradation of MB dye was monitored without ZnO NPs and only 11% degradation occurred within 60 min (figure 5(A)), whereas 98.11% of MB dye was degraded with photocatalyst ZnO NPs within 60 min under UV irradiation (figure 5(B)). Diallo *et al* [36] also reported degradation of MB and Congo red dyes in the presence of UV irradiation using ZnO NPs as photocatalyst. The present degradation results are compared with other reported literatures (table 2). Figure 5(C) shows degradation of MB dye ( $10 \text{ mg l}^{-1}$ ) with varying catalyst dose (10 mg, 20 mg, 30 mg). The photodegradation efficiency of MB dye was increased from 97.98 to 99.42 with increasing catalyst doses (10 to 30 mg). Photocatalytic dye degradation followed a pseudo first order kinetics model as calculated by the following equation as

$$r = \frac{dC}{dt} = kKC / (1 + KC)$$

Where, r is the degradation rate of dye, C is the concentration of dye solution, K is the adsorption coefficient of dye, t is the time of sampling during the degradation, and k is the reaction rate constant. Also, Venkata Reddy *et al* [37] reported degradation of Rh-B dye under UV irradiation, whereas Ranjan *et al* [38] reported photodegradation of MB dye by ZnO NPs as photocatalyst and found that the value of rate constant increased with increasing catalyst dose (table 3). When the initial concentration of dye solution was increased from  $5 \text{ mg l}^{-1}$  to  $15 \text{ mg l}^{-1}$ , the removal rate of dyes decreased from 98.84% to 97.63% for MB which is not so significant (figure 5(D), table 3).

#### Photodegradation of methyl orange (MO)

Figure 6(A) shows the photocatalytic dye degradation of MO in the presence of ZnO NPs as photocatalyst under UV irradiation ( $\lambda = 254 \text{ nm}$ ) and  $\lambda_{\text{max}}$  of MO dye is 462 nm in UV-visible spectrum. Only 8% degradation of MO happened without ZnO NPs photocatalyst within 100 min under UV irradiation (figure 6(A)), whereas 97.45% MO was degraded within 100 min with ZnO NPs as photocatalyst under UV irradiation (figure 6(B)). The obtained results of this study are resembled well with other reported literatures on MO dye degradation study (table 2). Figure 6(C) shows degradation of MO dye ( $10 \text{ mg l}^{-1}$ ) with varying catalyst dose (10 mg, 20 mg,

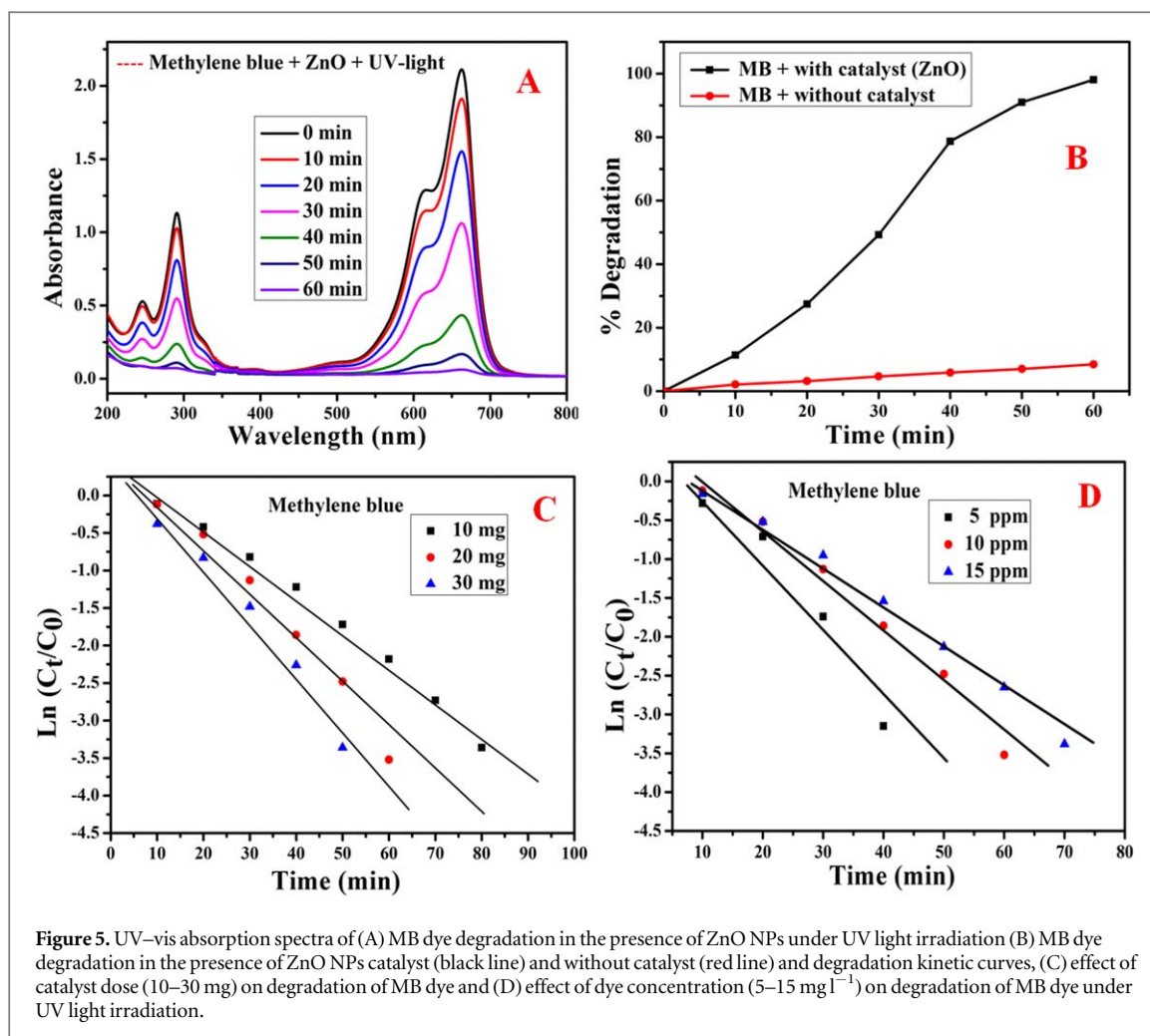


**Figure 5.** UV–vis absorption spectra of (A) MB dye degradation in the presence of ZnO NPs under UV light irradiation (B) MB dye degradation in the presence of ZnO NPs catalyst (black line) and without catalyst (red line) and degradation kinetic curves, (C) effect of catalyst dose (10–30 mg) on degradation of MB dye and (D) effect of dye concentration (5–15 mg l<sup>-1</sup>) on degradation of MB dye under UV light irradiation.

and 30 mg). The photodegradation efficiency of MO dye was increased from 97.09% to 98.12% respectively (figure 6(C)). When the initial concentration of dye solution was increased from 5 mg l<sup>-1</sup> to 15 mg l<sup>-1</sup>, the removal rate of dyes decreased slightly from 98.04% to 96.54% for MO (figure 6(D), table 3). Our results supported the findings of Kaur *et al* [51], because high concentrated dye molecules blocked majority active sites of catalyst, the adsorption of O<sub>2</sub> and OH on the photocatalyst was decreased leading to less generation of radicals. Also, the present study results are similar to *Eucalyptus globules* L. plant mediated synthesized ZnO NPs based MB and MO dyes degradation in the presence of UV light irradiation [52].

The present obtained results are compared with the results available in literatures [39–50] (table 2). It is clearly evident that the degradation time depends on the ratio of ZnO nanocatalyst dose (mg) to dye dose (mg), size and shape of nanoparticles (table 2). These reports suggest interaction of dyes with reactive oxygen species (ROS) generated *in situ* by nanomaterials in degrading MB and MO dyes [39–50]. Comparatively ZnO nanocatalyst exhibited enhanced degradation efficiency compared to others (table 2) which may be due to smaller nanoparticles size. MB degraded within 60 min with a rate constant of 0.14263 min<sup>-1</sup>, while MO degraded within 100 min with a rate constant of 0.22605 min<sup>-1</sup> (table 3).

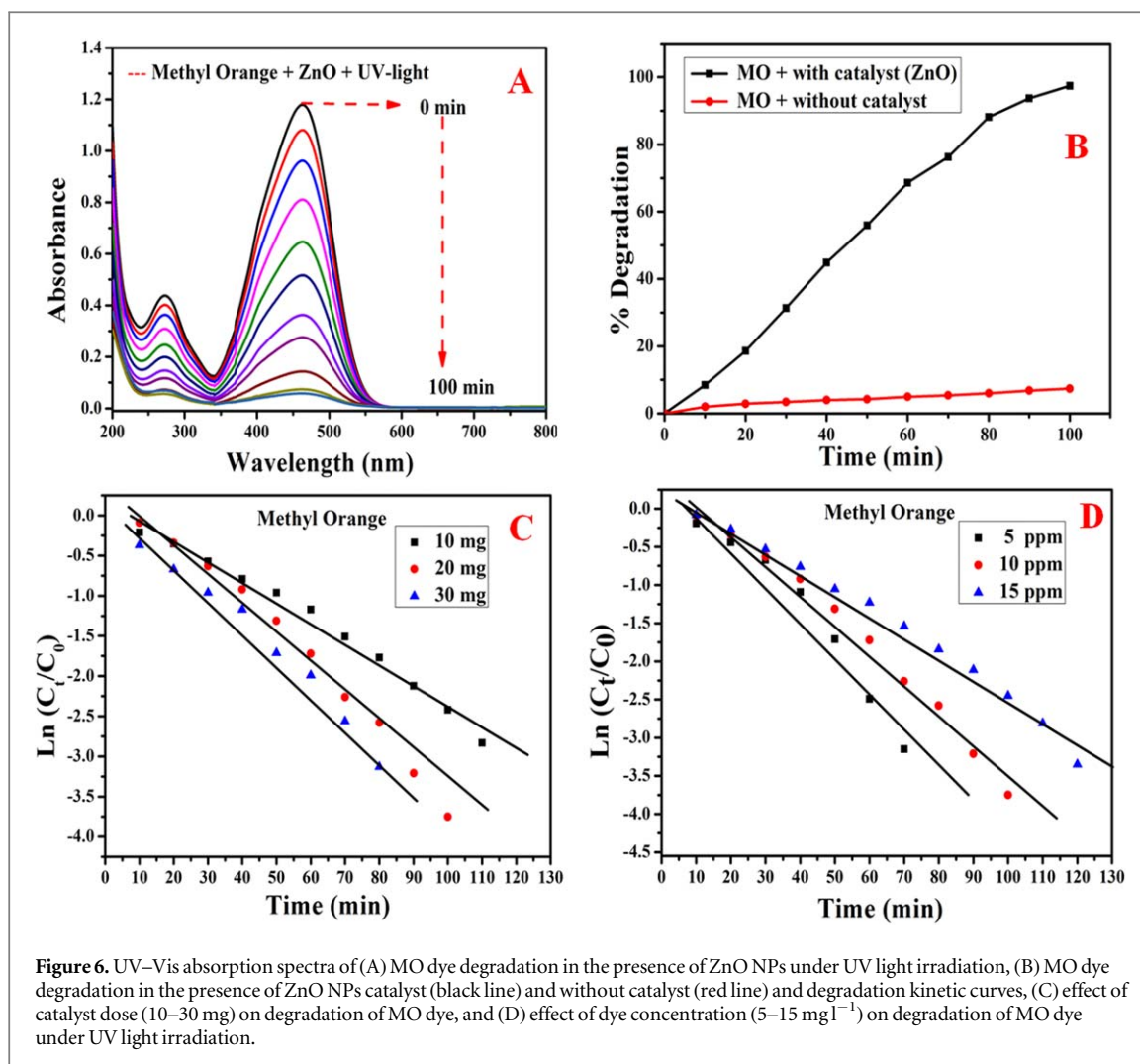
### Possible mechanism of dye degradation

The plausible mechanism of dye degradation using semiconductor ZnO NPs as photocatalyst towards degradation of MB or MO is predicted as follows:



**Table 2.** Photocatalytic activity of ZnO NPs to methylene blue (MB) and methyl orange (MO) dye degradation.

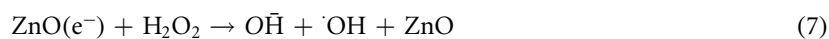
Dyes	Material used	NPs dose/dye dose	Size/shape	Time	Degradation efficiency (%)	References
MB	ZnO Nano-catalyst	312.69	14–70 nm/spherical shape	180 min	—	[39]
	Spindle-Like TiO <sub>2</sub>	100.00	50–70 nm/Spindle-Like	120 min	62.70% MB	[40]
	CuO microspheres	33.33	31 nm/flower-shaped	360 min	95.03% MB	[41]
	Sr doped ZnO Nano-catalyst	33.33	25–45 nm /hexagonal shapes	120 min	78.50% MB	[42]
	ZnO + rGO Nano-catalyst	33.33	15–35 nm/spherical shape	120 min	92.50% MB	[43]
	Cu/MMT Nano-catalyst	31.26	8 nm/spherical shape	120 min	95.06% MB	[44]
	ZnO- Nano-catalyst	33.33	17.25 nm/spherical shape	60 min	98.11% MB	Present work
MO	ZnO- Nano-catalyst	200.00	40–50 nm/needle shaped	140 min	95.40% MO	[45]
	SnO <sub>2</sub> Nano-catalyst	100.00	10–42 nm/spherical shape	120 min	94.00% MO	[46]
	ZnO Nano-catalyst	100.00	40 nm/spherical shape	120 min	83.99% MO	[47]
	TiO <sub>2</sub> Nano-catalyst	50.00	55 nm/spherical shape	210 min	71.50% MO	[48]
	NiFe <sub>2</sub> O <sub>4</sub> nano-catalyst	50.00	34.74 nm/quasi globular-shaped	300 min	72.66% MO	[49]
	Fe Nano-catalyst	12.00	7–14 nm/tetragonal shaped	100 min	95.00% MO	[50]
	ZnO- Nano-catalyst	33.33	17.25 nm/spherical shape	100 min	97.45% MO	Present work

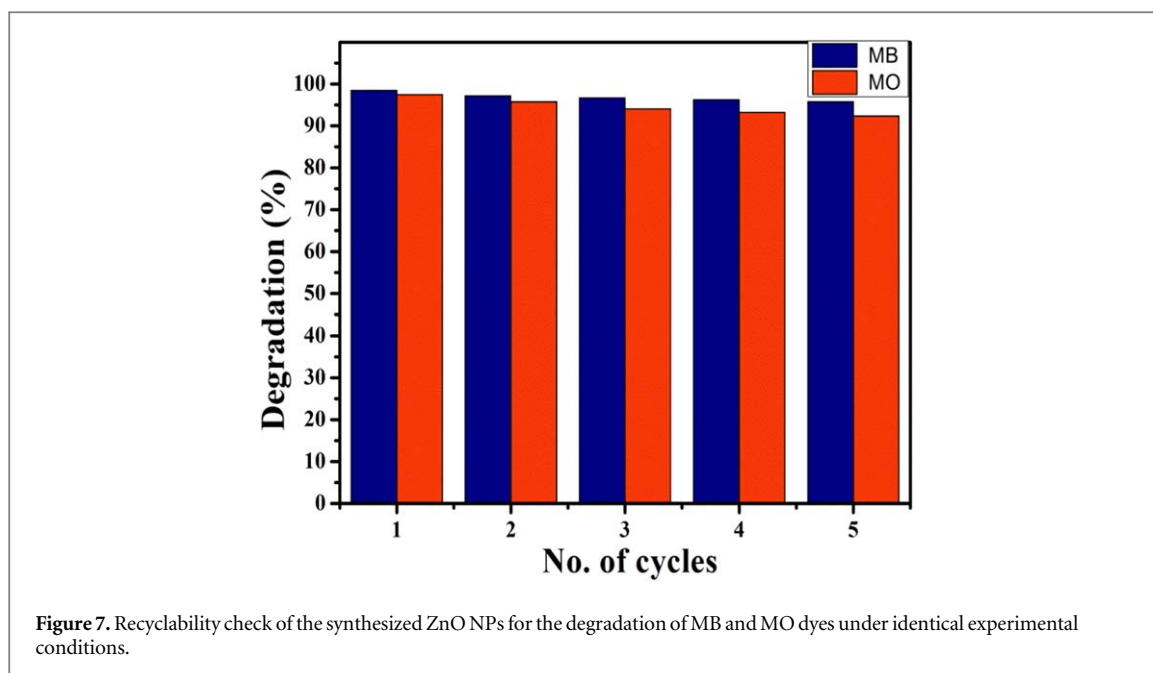


**Figure 6.** UV–Vis absorption spectra of (A) MO dye degradation in the presence of ZnO NPs under UV light irradiation, (B) MO dye degradation in the presence of ZnO NPs catalyst (black line) and without catalyst (red line) and degradation kinetic curves, (C) effect of catalyst dose (10–30 mg) on degradation of MO dye, and (D) effect of dye concentration (5–15 mg l<sup>-1</sup>) on degradation of MO dye under UV light irradiation.

**Table 3.** Degradation (%) and rate constant of MB and MO dye with ratio of catalyst dose (mg) to dye dose (mg).

Dye name	NPs dose (mg) /dye dose (mg)	Time (min)	Degradation (%)	Rate constant min <sup>-1</sup>
MB	16.66	80	97.98	0.08546
	33.33	60	98.11	0.14263
	50.00	50	99.42	0.22911
	66.66	40	98.84	0.24252
	33.33	60	98.11	0.14263
MO	22.22	70	97.63	0.07227
	16.66	110	97.09	0.12942
	33.33	100	97.45	0.22605
	50.00	80	98.12	0.35426
	66.66	70	98.04	0.34087
	33.33	100	97.45	0.22605
	22.22	120	96.54	0.15418





here... MB = Methyleme blue  
MO = Methyl Orange

↓  
degradation product (9)

When UV light was irradiation on ZnO NPs (2.89 eV), reactive oxygen species (ROS) was generated *in situ* which sequentially interacted with dyes and degraded to carbon dioxide and water molecules. Ajmal *et al* [53] proposed similar mechanism for TiO<sub>2</sub> NPs photocatalyst mediated dye degradation. When ZnO NPs is irradiated with UV light, conduction band gets electrons from valence band (equation (1)). The conduction band electron ( $\bar{e}_{CB}$ ) reacts with oxygen to produce the super oxide radical ions ( $\bar{O}_2$ ) (equation (2)) which react with hydrogen ions ( $H^+$ ) to produce peroxide ions ( $-OOH$ ) (equation (4)), whereas valence band holes ( $h_{VB}^+$ ) react with water molecules to release hydroxyl ions which then releases hydroxyl radicals (equations (3) and (5)). On the other hand the  $-OOH$  reacts with CB electrons and  $H^+$  ions to generate  $H_2O_2$  which consequently produce hydroxyl radical ( $\cdot OH$ ). The photoelectrons reduce  $O_2$  adsorbed on the photocatalyst surface into  $\bar{O}_2$ . Finally dyes were degraded by interacting with hydroxyl radicals ( $\cdot OH$ ) and superoxide radicals ( $\bar{O}_2$ ) to produce carbon dioxide and water molecules (equation (6)–(9)). Figure S3 shows possible reaction mechanism of MB and MO dye degradation in the presence of photocatalyst ZnO NPs under UV irradiation. Here the semiconductor ZnO NPs catalysed the redox reaction in the presence of air/ $O_2$  and water leading to complete mineralization of organic pollutants. Zangeneh *et al* [54] proposed similar radical mechanism for photocatalyst mediated dye degradation.

#### Reusability of the synthesized ZnO NPs

Recyclability test for the degradation of MB and MO dyes was done to evaluate the stability or performance of the prepared ZnO NPs under similar experimental conditions. The photocatalytic dye degradation experiments were repeated five times with 20 mg catalyst in 60 ml dye solution ( $10 \text{ mg l}^{-1}$ ) under UV irradiation. For reusability experiments, the catalyst was collected from reaction mixture, carefully washed with deionised water and dried after each experiment. The results of recyclability experiments are shown in figure 7. The degradation efficiencies of MB for five consecutive cycles were 98.11%, 97.15%, 96.68% and 96.20%, 95.73% respectively and degradation efficiencies of MO were 97.45%, 95.76%, 94.06% and 93.22%, 92.37% respectively. The results show a slight decrease in photodegradation efficiency after each cycle which matched to the results of Ban *et al* [55]. However, the biosynthesized ZnO NPs exhibited good photocatalytic activity with high stability under UV irradiation after 5 cycles of experiment.

#### Antioxidant activity of ZnO nanoparticles

Nagajyothi *et al* [56] reported antioxidant activity of ZnO NPs using DPPH assay. Banerjee *et al* [57] performed antioxidant activity of bulk and nanostructured polyaniline nanofibers and nanostructured polyaniline fibres and showed higher free radical scavenging activity since ZnO NPs possess higher surface to volume ratio compared to its bulk form. Herein antioxidant activity of ZnO NPs and extract was checked by using standard DPPH test. The results obtained in the antioxidant assay show effective free radical scavenging capacity of ZnO NPs.

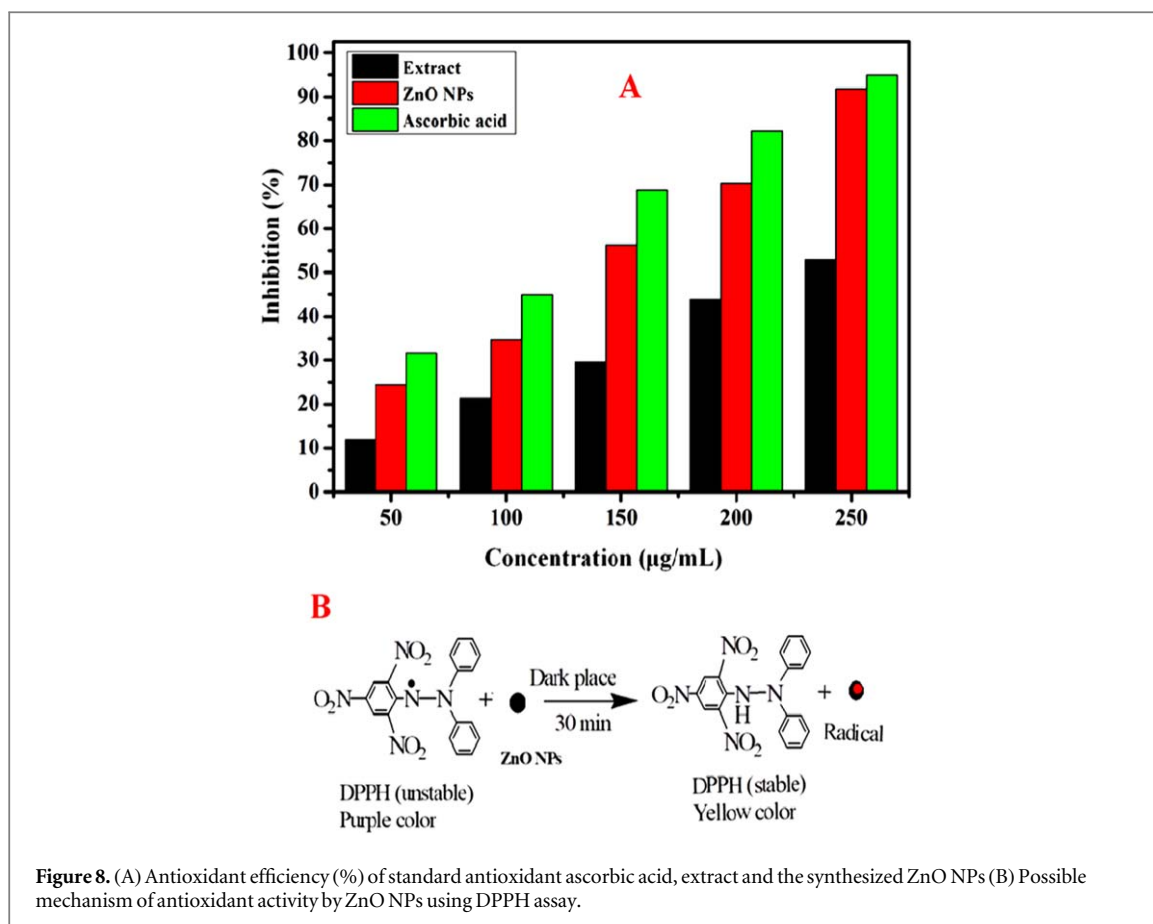


**Figure 8.** (A) Antioxidant efficiency (%) of standard antioxidant ascorbic acid, extract and the synthesized ZnO NPs (B) Possible mechanism of antioxidant activity by ZnO NPs using DPPH assay.

Figure 8(A) compares antioxidant activity of test samples with standard ascorbic acid by plotting different concentrations ( $\mu\text{g ml}^{-1}$ ) along  $x$ -axis versus scavenging inhibition (%) along  $y$ -axis. DPPH free radical scavenging capacity (%) increased from 21.44% to 91.85% with increasing photocatalyst ZnO NPs doses from  $50 \text{ mg l}^{-1}$  to  $250 \text{ mg l}^{-1}$  (figure 8(A)), whereas in the presence of extract scavenging capacity (%) increased from 11.94% to 54.79%. In a similar way we performed with standard ascorbic acid which shows the scavenging capacity (%) increased from 31.63% to 94.95% (figure 8(A)). The colour change of methanolic DPPH solution from purple to yellow was observed by the addition of ZnO NPs, because electron density of oxygen atoms in ZnO NPs was transferred to odd electron located at nitrogen atom in DPPH molecule i.e. this process increased the stability of DPPH molecule as well as increased the scavenging capacity of ZnO NPs. Also, the absorbance of the peak at 517 nm decreased which indicated the increasing free radical scavenging activity of ZnO NPs. Actually ZnO NPs being an electron donor, can convert free radicals to more stable products by terminating radical chain reaction [58]. Hence the reducing power of ZnO NPs is correlated well with the radical scavenging activity. Figure 8(B) shows the possible antioxidant mechanism of ZnO NPs in DPPH assay. In dark electron transfer from nanoparticles to 2,2-diphenyl-1-picrylhydrazyl molecules leads to stable 2,2-diphenyl-1-picrylhydrazine which proportionally varies with ZnO NPs dose [59].

## Conclusion

This reports 1st time on synthesis of ZnO NPs by using agro-waste durva grass aqueous extract. The synthesized nanocatalysts were characterized by UV-Vis, FTIR, powder XRD, HR-TEM, DLS and TGA analysis. The photocatalytic activity of ZnO NPs was studied for MB and MO dyes degradation with UV irradiation which was monitored by using UV-vis spectroscopy. MB degraded by 98.1% within 60 min, while 97.5% MO degraded within 100 min at a photocatalyst dose of  $10 \text{ mg l}^{-1}$ . As-synthesized ZnO NPs showed good photocatalytic activity as well as good antioxidant activity using DPPH assay against ascorbic acid as antioxidant standard. Hence the synthesized ZnO NPs could be considered as a good photocatalyst and antioxidant.

## Acknowledgments

The authors would like to thank Vellore Institute of Technology (VIT), Vellore - 632014 for the all-round support to do research works and instrumental facility for characterization of NPs.

## ORCID iDs

Badal Kumar Mandal  <https://orcid.org/0000-0003-2419-5247>

## References

- [1] Tuo Y, Liu G, Dong B, Zhou J, Wang A, Wang J and Jin R 2015 *Sci. Rep.* **5** 13515
- [2] Safar M, Raska I, Shor L M, Schrofel A, Kratosova G and Safar I 2014 *Acta Biomater.* **10** 4023–42
- [3] Chen H, Yu S M, Shin D W and Yoo J B 2010 *Nanoscale Res. Lett.* **5** 217–23
- [4] Komarneni S, Dong Y, Young J and Han S 2010 *Zeitschrift Fur Naturforsch. B* **65** 1033–7
- [5] Nejati K 2012 *Cryst. Res. Technol.* **47** 567–72
- [6] Zhu Y, Ji X, Wu Z, Song W, Hou H, Wu Z, He X, Chen Q and Banks C E 2014 *J. Power Sources.* **267** 888–900
- [7] Unni M, Uhl A M, Savliwala S, Savitzky B H, Dhavalikar R, Arnold D P, Kourkoutis L F, Andrew J S and Rinaldi C 2017 *ACS Nano.* **11** 2284–303
- [8] Gu F, Wang S F, Lu M K, Zhou G J, Xu D and Yuan D R 2004 *J. Phys. Chem. B* **108** 8119–23
- [9] Hu J, Dong Y, Ma Y, Ren C and Chen X 2014 *Chem. Eng. J.* **254** 514–23
- [10] Tiwari D K, Behari J and Sen P 2008 *World Appl. Sci. J.* **3** 417–33
- [11] Raliya R, Nair R, Chavalmane S, Wang W and Biswas P 2015 *Metallomics.* **7** 1584–94
- [12] Gangula A, Podila R, Ramakrishna M, Karanam L, Janardhana C and Rao A M 2011 *Langmuir* **27** 15268–74
- [13] Bala N, Saha S, Chakraborty M, Maiti M, Das S, Basu R and Nandy P 2015 *RSC Adv.* **5** 4993–5003
- [14] Sundrarajan M, Ambika S and Bharathi K 2015 *Adv. Powder Technol.* **26** 1294–9
- [15] Yan Y, Zhou Z, Li W, Zhu Y, Cheng Y, Zhao F and Zhou J 2014 *RSC Adv.* **4** 38558–67
- [16] Patel R and Suresh S 2006 *J. Hazard. Mater.* **137** 1729–41
- [17] Lin J, Zhao X, Liu D, Yu Z, Zhang Y and Xu H 2008 *J. Hazard. Mater.* **157** 541–6
- [18] Abid M F, Zablouk M A and Abid-alameer A M 2012 *Iranian J. Environ. Health Sci. Eng.* **9** 17
- [19] Ong S, Keng P, Lee W, Ha S and Hung Y 2011 *Water.* **3** 157–76
- [20] Li M, He W, Liu Y, Wu H, Wamer W G, Lo Y M and Yin J 2014 *J. Agric. Food Chem.* **62** 12052–60
- [21] Jin Z, Liu C, Qi K and Cui X 2017 *Sci. Rep.* **7** 39695
- [22] Mao B, An Q, Zhai B, Xiao Z and Zhai S 2016 *RSC Adv.* **6** 47761–70
- [23] Atarod M, Nasrollahzadeh M and Sajadi S M 2016 *J. Colloid Interface Sci.* **465** 249–58
- [24] Sutradhar P and Saha M 2015 *Bull. Mater. Sci.* **38** 653–7
- [25] Escobedo Morales A, Sanchez Mora E and Pal U 2007 *Rev. Mex. Fis.* **53** 18–22
- [26] Akbarian M, Mahjoub S, Elahi S M, Zabih E and Tashakkorian H 2018 *New J. Chem.* **42** 5822–33
- [27] Khodadadi B, Bordbar M and Nasrollahzadeh M 2017 *J. Colloid Interface Sci.* **493** 85–93
- [28] Sangeetha G, Rajeshwari S and Venkatesh R 2011 *Mater. Res. Bull.* **46** 2560–6
- [29] Raghupathi K R, Koodali R T and Manna A C 2011 *Langmuir* **27** 4020–8
- [30] Koupaei M H, Shareghi B, Ali Saboury A, Davar F, Semnani A and Evini M 2016 *RSC Adv.* **6** 42313–23
- [31] Wang L and Muhammed M 1999 *J. Mater. Chem.* **9** 2871–8
- [32] Suganthi K S and Rajan K S 2012 *Int. J. Heat Mass Transf.* **55** 7969–80
- [33] Moghaddam A B, Moniri M, Azizi S, Rahim R A, Bin Ariff A, Saad W Z, Namvar F, Navaderi M and Mohamad R 2017 *Molecules.* **22** 872
- [34] Ashkarran A A, Iradj Zad A, Mahdavi S M and Ahadian M M 2010 *Appl. Phys. A* **100** 1097–102
- [35] Gregg S J, Sing K S and Adsorption W 1982 *Surface Area and Porosity* 2nd edn (Academic Press INC) 66–29432
- [36] Diallo A, Manikandan E, Rajendran V and Maaza M 2016 *J. Alloys Compd.* **681** 561–70
- [37] Venkata C, Babu B, Vattikuti S V P and Ravikumar R V S S N 2016 *J. Lumin.* **179** 26–34
- [38] Ranjan P, Kamal R, Suematsu H, Phillip L and Sarathi R 2017 *J. Environ. Chem. Eng.* **5** 1676–84
- [39] Stan M, Popa A, Toloman D, Dehelean A, Lung I and Katona G 2015 *Mater. Sci. Semicond. Process.* **39** 23–9
- [40] Arunkumar S and Alagiri M 2017 *J. Clust. Sci.* **28** 2635–43
- [41] Mageshwari K, Sathyamoorthy R and Park J 2015 *Powder Technol.* **278** 150–6
- [42] Yousefi R, Jamali-Sheini F, Cheraghizade M and Khosravi-Gandomani S 2015 *Mater. Sci. Semicond. Process.* **32** 152–9
- [43] Azarang M, Shuhaimi A, Yousefi R and Jahromi S P 2015 *RSC Adv.* **5** 21888–96
- [44] Mekewi M A, Darwish A S, Amin M S, Eshaq G and Bourazan H A 2016 *Egypt. J. Pet.* **25** 269–79
- [45] Tripathy N, Eun J, Ah H and Hahn Y 2014 *Mater. Lett.* **136** 171–4
- [46] Srivastava N and Mukhopadhyay M 2014 *Ind. Eng. Chem. Res.* **53** 13971–9
- [47] Karnan T and Selvakumar S A S 2016 *J. Mol. Struct.* **1125** 358–65
- [48] Farbod M and Khademalrasool M 2011 *Powder Technol.* **214** 344–8
- [49] Hirthna, Sendhlnathan S, Rajan P I and Adinaveen T 2018 *J. Supercond. Nov. Magn.* **31** 3315–22
- [50] Radini I A, Hasan N, Malik M A and Khan Z 2018 *J. Photochem. Photobiol. B* **183** 154–63
- [51] Kaur S, Sharma S, Umar A, Singh S, Mehta S K and Kumar S 2017 *Superlattices Microstruct.* **103** 365–75
- [52] Reddy S B and Mandal B K 2017 *Adv. Powder Technol.* **28** 785–97
- [53] Ajmal A, Majeed I, Malik R N, Idriss H and Nadeem M A 2014 *RSC Adv.* **4** 37003–26
- [54] Zangeneh H, Zinatizadeh A A L, Habibi M, Akia M and Isa H M 2015 *J. Ind. Eng. Chem.* **26** 1–36
- [55] Ban J, Xu G, Zhang L, Lin H, Sun Z, Lv Y and Jia D 2017 *J. Solid State Chem.* **256** 151–7
- [56] Nagajyothi P C, Sreekanth T V M, Tettey C O, In Y and Heung S 2014 *Bioorg. Med. Chem. Lett.* **24** 4298–303
- [57] Banerjee S, Saikia J P, Kumar A and Konwar B K 2009 *Nanotechnol.* **21** 045101
- [58] Alam M N, Bristi N J and Rafiqzama M 2013 *Saudi Pharm. J.* **21** 143–52
- [59] Sonane M, Moin N and Satish A 2017 *Chemosphere.* **187** 240–7